EI SEVIER

Contents lists available at ScienceDirect

### International Journal of Mass Spectrometry

journal homepage: www.elsevier.com/locate/ijms



# pH dependent chelation study of Zn(II) and Ni(II) by a series of hexapeptides using electrospray ionization — Ion mobility — Mass spectrometry



Ayobami B. Ilesanmi, Tessa C. Moore, Laurence A. Angel \*

Department of Chemistry, Texas A&M University-Commerce, Commerce, TX, 75428, USA

#### ARTICLE INFO

Article history:
Received 17 April 2020
Received in revised form
19 May 2020
Accepted 20 May 2020
Available online 11 June 2020

Keywords:
His-Cys peptides
Zinc(II)-peptide complexes
Nickel(II)-peptide complexes
Cysteine metal binding
Matrix metalloproteinase inhibitors
Peptide tags

#### ABSTRACT

Presented here are the results of a study characterizing the selective metal chelating performance of the alternative metal binding (amb) peptide: acetyl-His1-Cys2-Gly3-Pro4-His5-Cys6-OH, and eight ambs with systematic modifications to His, Cys, and carboxyl C-terminus metal chelating sites. The results show that from the divalent metal ions of zinc, nickel, cobalt, magnesium and calcium, the ambs most extensively formed complexes with zinc and nickel. The ambs, which retained both Cys2 and Cys6 in their primary structure, exhibited the greatest formation of zinc complexes. The replacement of His<sub>1</sub> and His<sub>5</sub> residues with two additional Cys with the amidation of the C-terminus also increased the zinc chelation at pH 7.0. Density functional theory indicated that these modifications might be disrupting the hydrogen bonding between the His-Cys and carboxylate terminus making the 4Cys more available for chelation. Nickel chelation was generally lower than zinc because of competition from the Cys to form disulfide bonds in the presence of nickel. The two ambs that formed the highest number of nickel complexes both included the amidated C-termini and either 4Cys or 2Cys-2His. Comparison with recent published results of six heptapeptide ambs, which have the same primary structures, but with the inclusion of Tyr<sub>5</sub> before the final two residues, indicates the inclusion of the Tyr5 residue increases the zinc chelation at pH 7.0 from 25%, of total observed species, to 70%. These types of studies may pave the way to discoveries of new therapeutics suitable as enzyme inhibitors or chelators for diseases associated with metal homeostasis misbalances, or as new peptide tags for recombinant protein purification.

© 2020 Elsevier B.V. All rights reserved.

#### 1. Introduction

Zinc, nickel and cobalt ions are incorporated as cofactors into the proteins of living cells and are involved with biochemical functions such as metabolism, electron transport, oxidative protection, ATP synthesis, and genome reading [1]. At the active site of the protein, metal chelating groups such as imidazole of His, thiolate of Cys, and carboxylate of Glu or Asp [2,3] bind these metals. An intriguing question is how these ligands selectively incorporate different metal ions to ensure correct functioning.

Investigating the secondary and tertiary structures of metallopeptides by NMR spectroscopy or X-ray crystallography can provide atomic resolution. However, the NMR interpretation is

E-mail address: Laurence.Angel@tamuc.edu (L.A. Angel).

complicated or misinterpreted when multiple species are present in solution [4], and X-ray diffraction studies are scarce due to problems with the crystallization of metallopeptides [5]. An alternative technique that can overcome these problems is electrospray ionization - ion mobility - mass spectrometry (ESI-IM-MS). Previous ESI-IM-MS studies of peptide or protein complexes of zinc, nickel or cobalt include zinc finger peptides [6,7], His-rich glycoprotein [8], lysozyme [9], polyalanines [10,11], angiotensin I [12], insulin [13,14], Aβ1-40 peptide [15], and oxytocin [16,17]. Discrimination between specific and non-specific metal binding by proteins or peptides, observed during ESI-MS, has also been a focus of these studies [9,18-20]. Studies of alternative metal binding (amb) peptides [21-28] and methanobactin [29,30] from Methylosinus trichosporium (mb-OB3b) have shown that modulating the pH of the electrosprayed solution results in a pH-dependent formation of the metal complexes observed by ESI-IM-MS. The primary structures of the amb peptides include Pro as a hinge to position the His and Cys substituent groups for coordinating the

 $<sup>\</sup>ast$  Corresponding author. Department of Chemistry, Texas A&M University-Commerce, 2600 S Neal St., Commerce, TX, 75428, USA.

metal ion (Fig. 1). These studies have shown that ESI-IM-MS analyses correlate to the weak acid-base nature of the Cys and His substituent groups because the metal coordination increases when the pH of their two respective pKas has been reached. The measured m/z and collision cross section in negative ion mode is particularly informative because it exhibits a distinct pH dependence for the metal binding and provides the protonation state of the acidic and basic sites, the charge of the metal ion(s), the number of disulfide bonds, separation of isobaric oligomers, and the size and shape of the conformer.

Designing bioactive peptides is a key component for understanding peptide folding and metal ions preference for the primary structure of oligopeptides. Metal-chelating agents have applications as therapeutics for diseases that originate from metal ion or enzyme activity misbalances. For example, matrix metalloproteinases (MMP) contain the zinc(II) cofactor to catalyze the hydrolysis of structural proteins in the extracellular matrix [31], and misbalance of MMP activity have been related to the dissemination and metastasis of cancers [32]. As a result, MMP inhibitors have been designed to bind to the active site and zinc(II) cofactor to inhibit their hydrolysis function [31,33,34]. The zinc(II) and hydrogen bonding interactions of the ambs make them promising MMP inhibitors [23,25,27]. The design of new heterogeneous peptide tags for recombinant protein purification via immobilized metal affinity chromatography (IMAC) is another application. Cobalt, zinc and nickel are the most commonly used metal ions for IMAC purification with the hexa-His tag. The lack of heterogeneity in hexa-His tag however, leads to problems in toxicity, distribution and solubility in the expression of the recombinant protein in the bacterium cell [35]. To develop chelators with optimal capabilities for binding selected metal ions, nine amb<sub>1</sub> hexapeptides (1A to 1I, Fig. 1) were designed and synthesized to investigate their effectiveness using the His, Cys and C-terminus carboxylate for chelating the metal (II) ions of zinc, nickel, cobalt, magnesium and calcium at pH 6.7–9.4. Magnesium and calcium were included in the study because of their high availability in biological fluids and to test whether these ions would compete with the transition metal binding. Our previous study of  $amb_{1A}^{21}$  showed that it would bind with Zn(II) and Ni(II) but not with Mn(II), Fe(II) or Co(II). This current study, also allows comparison with the results of a recent metal-binding study of a series of amb<sub>5</sub> heptapeptides, 5A to 5F [23,25,27], which were designed and synthesized with similar amino acid sequences to 1A to 1F, but with the addition of the Tyr<sub>5</sub> residue at position-5 in their primary structure (Fig. 1).

### 2. Experimental section

### 2.1. Reagents and working solutions

The alternative metal binding-1 (amb<sub>1</sub>) peptides **1A-1I** were synthesized by PepmicCo (http://www.pepmic.com/). Ammonium acetate (ultra pure) was purchased from VWR (https://us.vwr.com/) and nickel (II) nitrate hexahydrate (99% purity) was purchased from ACROS (https://www.acros.com/). Ammonium hydroxide (trace metal grade), calcium nitrate tetrahydrate (ACS grade), and magnesium nitrate hexahydrate (ACS grade) were purchased from Fisher Scientific (http://www.Fishersci.com/). Zinc nitrate hexahydrate (99%+ purity) was purchased from Alfa Aesar (www.alfa.com/). Cobalt (II) acetate (99.99%) were purchased from Sigma-Aldrich (www.sigmaaldrich.com/). All working solutions were prepared with >17.8 M $\Omega$  cm deionized (DI) water (http://www.millipore.com).

### 2.2. Sample preparation and ion mobility — mass spectrometry analysis

Individual samples were prepared containing one of the amb\_1 peptides, pH adjusted with ammonium acetate/ammonium hydroxide solution, before an equimolar amount of the metal ion added and mixed aerobically at room temperature. The final solutions for ESI-IM-MS analysis contained both the amb\_1 and metal ion at 12.5  $\mu\text{M}$  and the ammonium acetate/ammonium hydroxide to modify the pH. The total ionic strength of these solutions were 9.0 mM for pH 7.0, 13 mM for pH 8.3, and 60 mM at pH 9.4. Solutions were left at room temp for 10 min before half of the sample was electrosprayed into the Waters Synapt HDMS (G1) [36] and the other half was used to measure the final pH. The tuned ESI and IM conditions limit any structural rearrangement or dissociation of the amb\_1 species, with the typical operating conditions described in the supporting information.

### 2.3. Analysis of the metal:amb<sub>1</sub> ESI-IM-MS data

All positively- and negatively-charged ions were identified by their m/z isotope patterns and their arrival time distributions (ATDs) extracted using Driftscope 2.0. The centroid and the area under the ATD curve were determined using MassLynx 4.1. From the centroid the collision cross section (CCS<sub>He</sub>) was determined using a calibration method with drift-tube CCS<sub>He</sub> values of polyalanine standards measured in helium buffer gas [37] as described

```
amb<sub>1A-I</sub>
(1A) ac-His-Cys-Gly-Pro-His-Cys-OH
                                                                                        Pro<sub>4</sub>
                                                                                                  amb<sub>5A-F</sub>
(1B) ac-His-Cys-Gly-Pro-His-Cys-NH<sub>2</sub>
                                                                                                  (5A) ac-His-Cys-Gly-Pro-Tyr-His-Cys-OH
(1C) ac-His-Cys-Gly-Pro-Gly-Cys-OH
                                                                                                  (5B) ac-His-Cys-Gly-Pro-Tyr-His-Cys-NH<sub>2</sub>
(1D) ac-Gly-Cys-Gly-Pro-Gly-Cys-OH
                                                                                                  (5C) ac-His-Cys-Gly-Pro-Tyr-Gly-Cys-OH
(1E) ac-His-Gly-Gly-Pro-His-Cys-OH
                                                                                                  (5D) ac-Gly-Cys-Gly-Pro-Tyr-Gly-Cys-OH
(1F) ac-His-Gly-Gly-Pro-His-Gly-OH
                                                                                                  (5E) ac-His-Gly-Gly-Pro-Tyr-His-Cys-OH
(1G) ac-Cys-Cys-Gly-Pro-Cys-Cys-NH<sub>2</sub>
                                                                                                  (5F) ac-His-Gly-Gly-Pro-Tyr-His-Gly-OH
(1H) ac-His-Gly-Gly-Pro-Gly-Gly-OH
(11) ac-His-Gly-Gly-Pro-Gly-Gly-NH2
                                                     His_1
                                          Acetyl
```

Fig. 1. The predicted structure of the neutral charged state of the alternative metal binding-1A (amb<sub>1A</sub>) peptide showing the potential binding sites of the 2His-2Cys substituent groups (shaded in brown ), and the proline (shaded in blue ) which forms the tight turn. The comparison of the primary structure of (1A) amb<sub>1A</sub> with the other amb<sub>1</sub> peptides studied here are shown (1B) amb<sub>1B</sub> (1C) amb<sub>1C</sub> (1D) amb<sub>5D</sub> (1E) amb<sub>5E</sub> (1F) amb<sub>5E</sub> (1G) amb<sub>1G</sub> (1H) amb<sub>1H</sub> and (1I) amb<sub>1I</sub>. The primary structures of the previously studied heptapeptides, amb<sub>5A-E</sub> are also shown (5A-5F).

in the supporting information. The area under each ATD curve determined the relative intensity of each species in the pH adjusted sample by normalizing their area to the sum of the areas of all amb<sub>1</sub> species identified in that sample. The bar graphs showing the contribution from both the positively- and negatively-charged complexes were re-normalized to the percentage scale by halving the contribution from each charge state. The relative percentage scale was used to account for any bias in the ESI efficiency for transferring the peptides into the gas-phase and by including both positive and negative ion analyses, the propensity of the peptides for forming either positive or negative ions was also taken into account. The Zn(II) and Ni(II) binding experiments with 1A to 1I at pH 7, 8, and 9 were repeated three times each and showed standard deviations of between 2 and 15% for the relative percent intensity.

#### 2.4. Computational methods

The Becke three parameter hybrid functionals with the Def2 split-valence basis set [38,39], B3LYP/Def2SV, from Gaussian 09, [40] was used to locate the lowest energy, geometry optimized, gasphase conformers of the amb<sub>1</sub> Ni(II) or Zn(II) complexes containing only trans-peptide bonds. The Def2 basis set is recommended for DFT calculations on main group elements and first row transition metals (H-Kr) and is more reliable than the older LanL2DZ or the split-valence Pople basis sets. The study compared the different binding site combinations and protonation states of the 2Cys, 2His, and C-terminus groups, which combined with the charge of the metal ion to give the overall charge of the  $[amb_{1A/B}-3H + Ni(II)]^{-}$ and  $[amb_{1A}-3H + Zn(II)]^-$  complexes. For comparison, the study located the lowest energy conformers for the distorted tetrahedral coordination of the metal via either 2Cys-2His, 2Cys-His-Cterm or Cys-2His-Cterm. The final located conformers exhibited the same deprotonation sites and binding geometries for both the Ni(II) and the Zn(II) complexes. For each metal complex, the geometry optimized conformers were all checked for 0 imaginary frequencies and their predicted free energies were given relative to the lowest energy conformer. The CCS<sub>He</sub> of each of the B3LYP/Def2SV conformers were calculated using the ion size scaled Lennard-Jones (L-J) method [41], using ten measurements to determine the mean and standard deviation of the L-J CCSHe.

### 3. Results and discussion

### 3.1. Metal(II)-binding between pH 6.7 to 9.4

Using the ESI-IM-MS gas-phase analyses of both negatively- and positively-charged ions, the selectivity for the  $amb_1$  peptides for binding the metal(II) ions of cobalt, zinc, nickel, magnesium, and calcium were tested over pH 6.7 to 9.4. Of these metal ions, only the nickel and zinc resulted in the formation of  $amb_1$  complexes >15% which increased in a pH-dependent manner over pH 6.7 to 9.4. The magnesium, calcium and cobalt exhibited <15% formation of  $amb_1$  complexes at the physiological pH 7.0 (Fig. S2), with only the higher oxidation state of cobalt(III) identified to bind to species **1E** and **1H** at pH 9.4 at > 15% (Fig. S3).

### 3.2. Formation of charged species from $amb_{1A-I} + Ni(II)$ over pH 6.7 to 9.4

Comparison of how changes in the primary structure of amb<sub>1A</sub> affected Ni(II) chelation was tested by both positive and negative ESI-IM-MS analyses of species **1A** to **1I** as a function of pH over 6.7 to 9.4. Interestingly, both positive and negative ion analyses showed a similar pH-dependence for the formation of the Ni(II) complexes, although the behavior was typically more distinct in the

negatively-charged analyses. Singly-charged negative ions were observed from the analyses of negative ions of **1A** to **1I** and both singly- and doubly-charged positive ions were observed from the positive ion analyses. In both cases, the overall charge was conserved by the charge of the metal(II) and by the loss or gain of protons, *e.g.*, for positive ions  $[amb_1+H]^+$ ,  $[amb_1+2H]^{2+}$ ,  $[amb_1-H+Ni(II)]^+$ , and  $[amb_1+Ni(II)]^2+$  (Fig. S4), and for negative ions  $[amb_1-H]^-$ ,  $[amb_1-3H+Ni(II)]^-$ . Samples of the negative ion mass spectra for Ni(II)-binding to  $amb_{1B}$  are shown in Fig. 2. The main observed species were the negatively-charged  $[amb_{1B}-H]^-$ ,  $[amb_{1Box}-H]^-$ , and  $[amb_{1B}-3H+Ni(II)]^-$ , where the ox subscript signifies oxidation through the formation of a disulfide bond between the two sulfurs of 2Cys.

The formation of negatively-charged species from Ni(II) and 1A to 11 are shown in Fig. 3, and at pH 7, the main species was [amb<sub>1</sub>-H]<sup>-</sup> for all ambs. At pH 8, there was an increase in the oxidation of the two Cys thiol groups resulting in the formation of a disulfide bond as shown by  $[amb_{1OX}-H]^-$  for 1A, 1B, 1C, and 1D. The extent of the disulfide bond formation was dependent on the presence of nickel, and has been previously observed and detailed for copper with amb peptides [21,22,24]. The amb<sub>1</sub> peptides did not form disulfide bonds in the pH range 7-9, without the addition of the Ni(II). The oxidation after the addition of Ni(II) indicates the metal is catalyzing the formation of the disulfide bonds. The Cys oxidation was greatest for species 1D, which does not contain either of the His substituent groups. Previous B3LYP modelling [25] of 5A predicted salt-bridges formed between the Cys thiolates and His imidazolium groups, exhibiting a tertiary structure L-I CCS<sub>He</sub> that agreed with the IM-MS measurement. However, for 1A the lowest energy conformer located using B3LYP/Def2SV in this new study exhibits 7 hydrogen bonds, with 4 of them involving the Cterminus carboxylate, and a hydrogen bond between His1 and Cys6 (Fig. S5). These His-Cys salt-bridges and hydrogen bond may lower the reactivity of Cys for forming the disulfide bond. Species 1E also formed a disulfide bond on the addition of Ni(II) but because it contained only one Cys in its primary structure it formed an intermolecular disulfide bond resulting in an oxidized dimer.

The most apparently reactive species for forming Ni(II) complexes was **1B**, which formed > 60% of  $[amb_{1B}-3H + Ni(II)]^{-}$  at pH 8.2 to 9.4. This indicated that Ni(II) chelation was associated with the availability of the 2Cys thiolates, 2His imidazoles and the amidated C-terminus. Evidence for the Ni(II) preference for the amidated C-terminus of 1B rather than the carboxyl C-terminus of 1A was observed by the lower 20% and 38% formation of  $[amb_{1A}-3H + Ni(II)]^{-}$  at pH 8.3 and 9.4, respectively. The higher formation of the Ni(II) complex for 1B may be also influenced by the increased pKa of the amidated C-terminus, lowering the efficiency of the disulfide bond reaction. The removal of one or more of the 2His and 2Cys substituent in the structures of 1C, 1D, 1E, 1F, 1H, and 1I, resulted in a decrease to <20% formation of the Ni(II) complexes, justifying the hypothesis that their substituent groups were involved in Ni(II) chelation. However, when the 2His were replaced with two more Cys and the C-terminus amidated, 1G, both singlyand doubly-charged complexes were observed coordinating one and two Ni(II) ions, indicating the 4Cys and C-terminus amide group could chelate up to 2Ni(II).

The complex  $[amb_1-3H + Ni(II)]^-$  has three sites that were deprotonated, which for species 1A and 1B could either be the 2Cys thiolates, the deprotonated C-terminus group, or the second deprotonation of one of the His forming a negatively charged imidazolate. Evidence for the Cys thiolates involvement in Ni(II) binding was further indicated because the oxidized species, with the disulfide bond, was not able to bind the Ni(II). The comparison of the negatively charged sites, discussed above, for Ni(II) coordination was investigated using B3LYP/Def2SV molecular modelling.

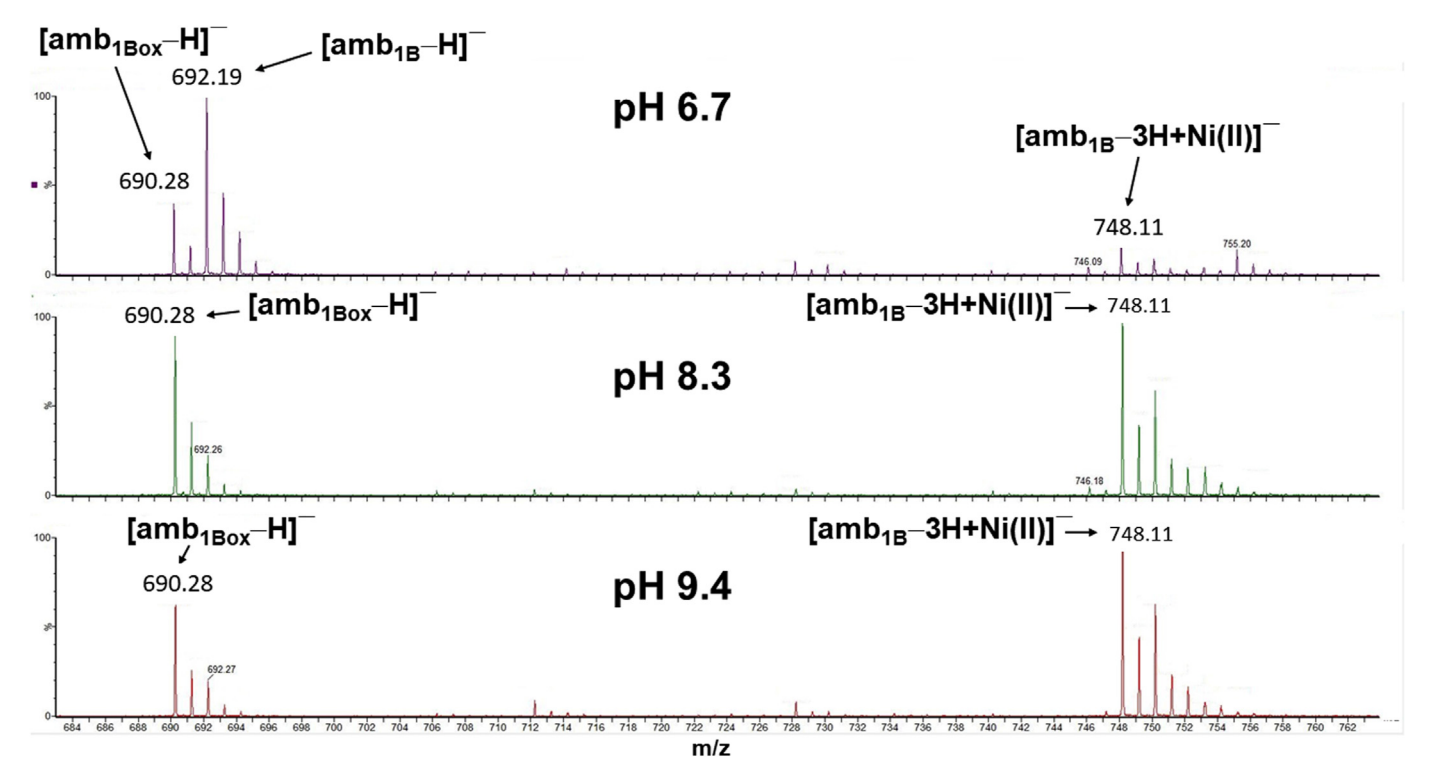


Fig. 2. The mass spectra showing the isotope patterns of the principal negatively-charged species observed from the equimolar solutions of Ni(II) and amb<sub>1B</sub> at pH 6.7, pH 8.3 and pH 9.4.

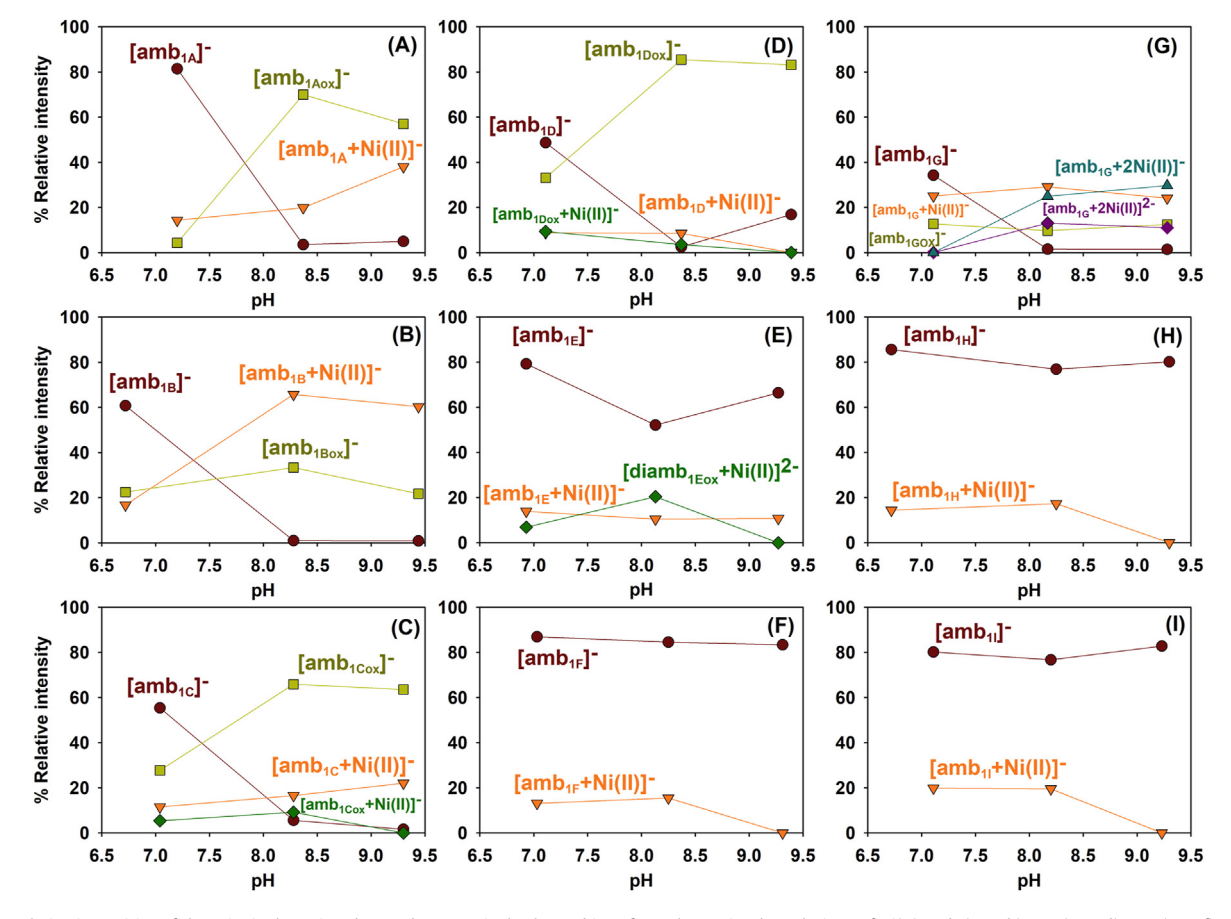


Fig. 3. The relative intensities of the principal species observed as negatively charged ions from the equimolar solutions of Ni(II) and a) 1A, b) 1B, c) 1C, d) 1D, e) 1E, f) 1F, g) 1G, h) 1H and i) 1I over pH 6.7 to 9.4. The relative intensities have standard deviations of 2–15%.

## 

**Fig. 4.** B3LYP/Def2SV lowest energy, geometry optimized conformers of Ni(II) coordination by amb<sub>1A</sub> via **a**) imidazole of His<sub>1</sub>, thiolate groups of Cys<sub>2</sub> and Cys<sub>6</sub> and C-terminus carboxylate group; **b**) imidazole of His<sub>1</sub>, thiolate of Cys<sub>2</sub>, imidazole of His<sub>5</sub>, and C-terminus carboxylate group; and **c**) imidazolate of His<sub>1</sub>, thiolate groups of Cys<sub>2</sub>, Cys<sub>6</sub> and imidazole of His<sub>5</sub>. The thermal free energies ( $\mathbf{G}$ ) are shown normalized to the lowest energy Ni(II) complex with the Lennard-Jones collision cross sections (L-J CCS<sub>He</sub>) for each coordination motif.

L-J  $CCS_{He} = 171 \pm 5 \text{ Å}^2$ 

Our investigations were directed by our extensive B3LYP modelling of the analogous amb<sub>5A-F</sub> (Fig. 1) [23,25,27]. These studies discovered that if all the peptide bonds were conserved as trans, including trans-Pro, the geometry optimized conformers were in much better agreement with the IM-MS measured CCSHe. The lowest energy trans-Pro conformers of 5A, 5B and 5C all exhibited His<sub>1</sub>-Cys<sub>2</sub>-Cys<sub>7</sub> and C-terminus metal coordination [25,27]. The trans-Pro conformers were over 88 kJ/mol higher in free energy than their lowest energy cis-Pro conformers [25], but because the amb<sub>1</sub> and amb<sub>5</sub> peptides are synthesized with trans-peptide bonds, the energy barrier for conversion to the cis-Pro must constrain its formation. The His<sub>1</sub>-Cys<sub>2</sub>-Cys<sub>7</sub> and C-terminus coordination was also consistent to why 5A, 5B, and 5C were the most effective Zn(II) or Ni(II) chelators because these chelating sites remained intact in these peptides, whereas, with 5D, 5E, and 5F these sites were replaced with Gly and the metal binding was adversely affected [25,27].

 $\text{L-J CCS}_{\text{He}} = 168 \pm 3 \text{ Å}^2$ 

Therefore, for this study we focused on the trans-Pro of 1A and because they exhibited the greatest formation of [amb<sub>1</sub>-3H + Ni(II)]<sup>-</sup>, with 3 deprotonation sites relating to the 2His, 2Cys and either the carboxyl or amide C-terminus groups. For a tetrahedral coordination, these sites can combine as either 2Cys-2His, 2Cys-His-Cterm or Cys-2His-Cterm in binding the Ni(II) and so our study located the lowest energy conformer of each of these binding motifs. The results of the B3LYP/Def2SV study predicted that for 1A the lowest energy complex of Ni(II) was the 2Cys-His-Cterm chelation through the His<sub>1</sub>, Cys<sub>2</sub>, Cys<sub>6</sub>, and C-terminus carboxyl group (Fig. 4a), with each Cys and the C-terminus carboxyl deprotonated. The Cys-2His-Cterm chelation through His<sub>1</sub>, Cys<sub>2</sub>, His5 and the C-terminus carboxyl coordination of Ni(II) was predicted to be 77.8 kJ/mol higher in energy (Fig. 4b), with each Cys and the C-terminal carboxyl deprotonated. The 2Cys-2His coordination of Ni(II) was 119 kJ/mol higher in energy (Fig. 4c) and was

L-J  $CCS_{He} = 174 \pm 2 \text{ Å}^2$ 

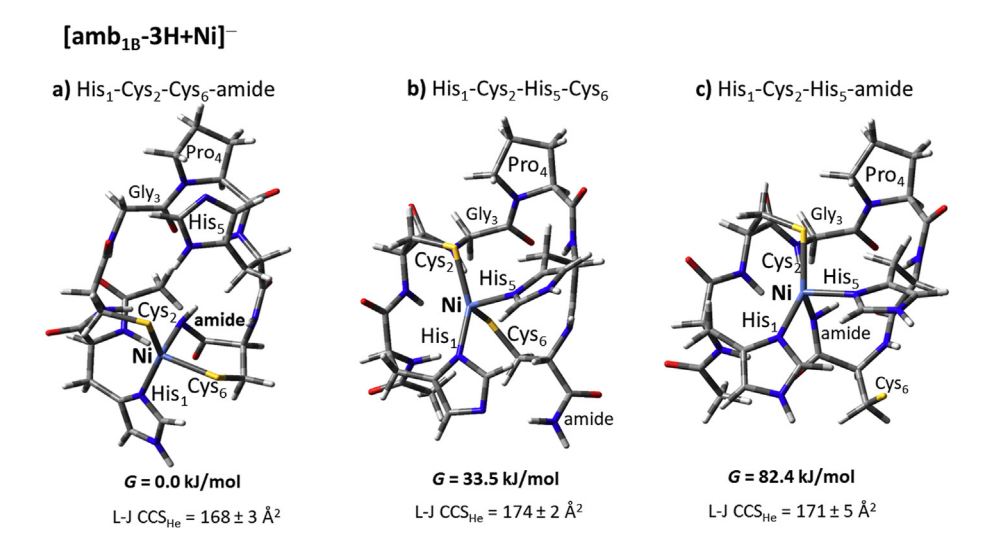


Fig. 5. B3LYP/Def2SV lowest energy, geometry optimized conformers of Ni(II) coordination by amb<sub>1B</sub> via **a**) imidazole of His<sub>1</sub>, thiolate groups of Cys<sub>2</sub> and Cys<sub>6</sub> and C-terminus amide group; **b**) imidazolate of His<sub>1</sub>, thiolate groups of Cys<sub>2</sub>, Cys<sub>6</sub> and imidazole of His<sub>5</sub>; and **c**) imidazole of His<sub>1</sub>, thiolate of Cys<sub>2</sub>, imidazole of His<sub>5</sub>, and C-terminus amide group. The thermal free energies (G) are shown normalized to the lowest energy Ni(II) complex with the Lennard-Jones collision cross sections (L-J CCS<sub>He</sub>) for each coordination motif.

**Table 1** Singly negatively-charged experimental IM-MS collision cross sections for free amb<sub>1</sub> **1A-1I** species and their Ni(II) and Zn(II) complexes with absolute uncertainties of 4  $\mathring{A}^2$  [37].

	Collision Cross Section, CCS <sub>He</sub> (Å <sup>2</sup> )								
Species	1A	1B	1C	1D	1E	1F	1G	1H	1I
[amb-H]	170	173	158	142	165	156	157	145	149
[amb-3H + Ni(II)]	173 <sup>a</sup>	175ª	161	146	168	161	161	149	152
[amb-3H + Zn(II)]	171ª	174 <sup>a</sup>	158	143	162	160	160	150	_

 $<sup>^</sup>a$  The theoretical L-J CCS $_{He}$  of 1A and 1B via 2Cys-His-Cterm  $=168\pm3$  Ų, Cys-2His-Cterm  $=171\pm5$  Ų, or 2Cys-2His  $=174\pm2$  Ų.

through the imidazolate of His<sub>1</sub>, thiolates of 2Cys, and imidazole of His<sub>5</sub>. Therefore, the B3LYP/Def2SV method predicted the same result as for the amb<sub>5</sub> peptides that the lowest energy coordination was via His<sub>1</sub>, Cys<sub>2</sub>, Cys<sub>6</sub> and C-terminus group. This was also true for **1B**, where the B3LYP/Def2SV method found the lowest energy Ni(II) coordination was through His<sub>1</sub>, Cys<sub>2</sub>, Cys<sub>6</sub> and the C-terminus amide (Fig. 5a). However, for **1B** the 2Cys-2His coordination (Fig. 5b) was predicted to be 33.5 kJ/mol higher in energy, whereas, the His<sub>1</sub>, Cys<sub>2</sub>, His<sub>5</sub> and the C-terminus coordination (Fig. 5c) was 82.4 kJ/mol higher in free energy. These results indicated that even though the C-terminus was amidated it can deprotonate and chelate the Ni(II). Therefore, all the **1B** conformers had the same analogous chelation and deprotonation sites as the **1A** complexes.

Table 1 shows the IM-MS measured  $CCS_{He}$  for the singly negatively-charged Ni(II) complexes of  $amb_{1A-I}$ . Comparison of  $\bf 1A$  and  $\bf 1B$  with the theoretical L-J  $CCS_{He}$  for the B3LYP conformers of  $[amb_{1A}-3H+Ni(II)]$  and  $[amb_{1B}-3H+Ni(II)]$  (Figs. 4 and 5) shows

there is agreement between the IM-MS  $CCS_{He}$  and L-J  $CCS_{He}$  of all three *trans*-Pro coordination types, within the associated uncertainties of both measurements. For species **1C** to **1I**, there is an observable trend in the changes of size of their conformations as the substituent groups of the His or Cys are systematically removed and replaced.

### 3.3. Formation of charged species from $amb_{1A\text{--}I} + Zn(II)$ over pH 6.7 to 9.4

The positive and negative ion analyses of  $amb_{1A-I} + Zn(II)$ showed pH-dependent formation of the Zn(II) complexes, which was more distinct in the negative ion analyses. The relative intensities of the negatively charged species of amb<sub>1</sub>+Zn(II) over pH 6.7 to 9.4 are shown in Fig. 6. Species 1A, 1B, 1C, and 1D, exhibited a similar pattern for the formation of  $[amb_1-3H + Zn(II)]^-$  complex, which indicates that the 2Cys were primarily responsible for their higher percentage of coordination of Zn(II) at pH 8.3-9.4. Unlike for the Ni(II), the formation of a disulfide bond was not a major channel for the  $amb_1+Zn(II)$ . In our previous studies [23] it was shown that B3LYP predicted that the lowest energy cis-Pro conformation of amb<sub>5A</sub> (**5A**, Fig. 1) coordinated the Zn(II) by a distorted tetrahedral via S of Cys<sub>2</sub>, backbone carbonyl O of Cys<sub>2</sub>, S of Cys<sub>7</sub>, and O of the carboxylate terminal group. However, the IM-MS measured CCS of  $[amb_{5A}-3H + Zn(II)]^{-}$  agreed much better with the lowest energy trans-Pro conformation of Zn(II), which was coordinated via the substituent groups of His1, Cys2, Cys7 and the C-terminus carboxvlate [25].

Likewise, the results of the B3LYP/Def2SV calculations for amb<sub>1A</sub>

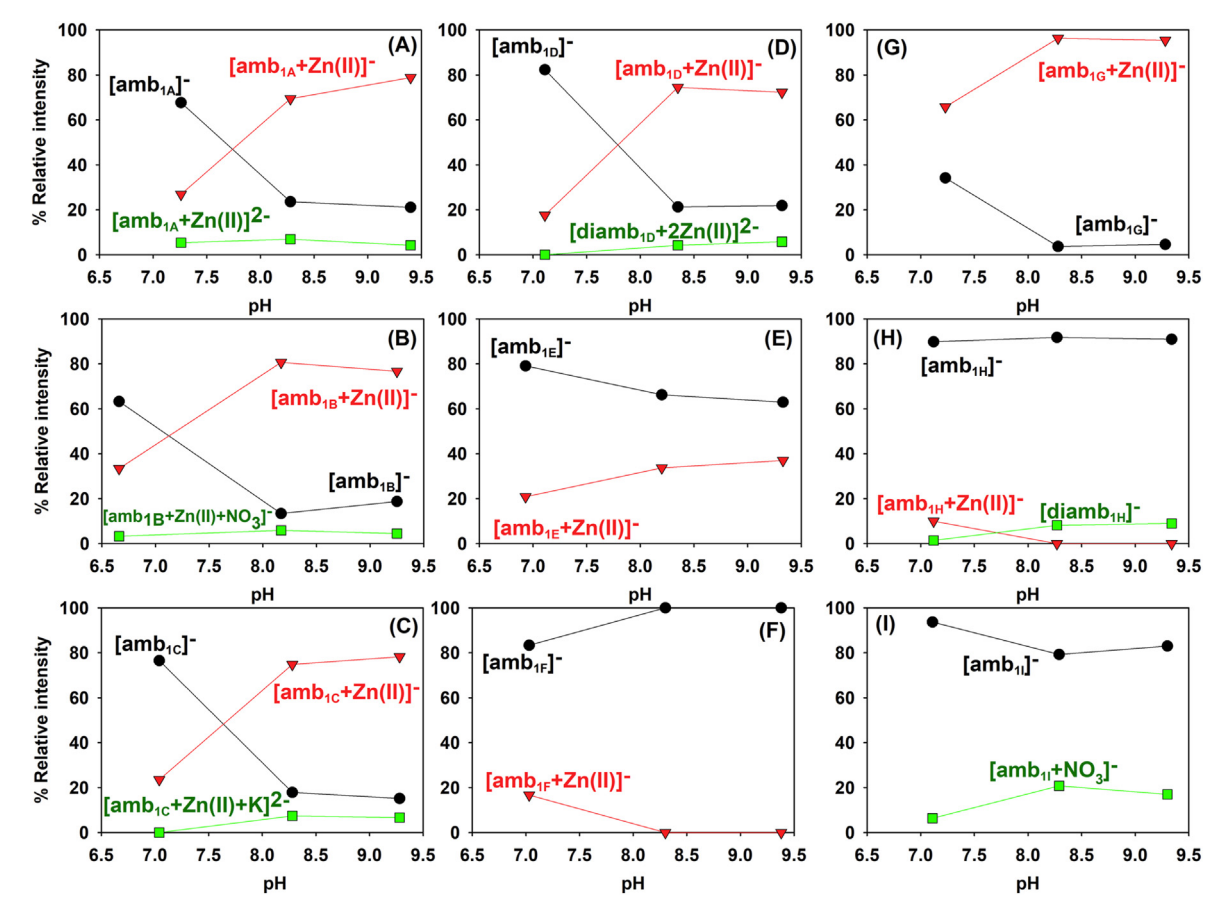


Fig. 6. The relative intensities of the principal species observed as negatively charged ions from the equimolar solutions of Zn(II) and a) 1A, b) 1B, c) 1C, d) 1D, e) 1E, f) 1F, g) 1G, h) 1H and i) 1I over pH 6.7 to 9.4. The relative intensities have standard deviations of 2–15%.

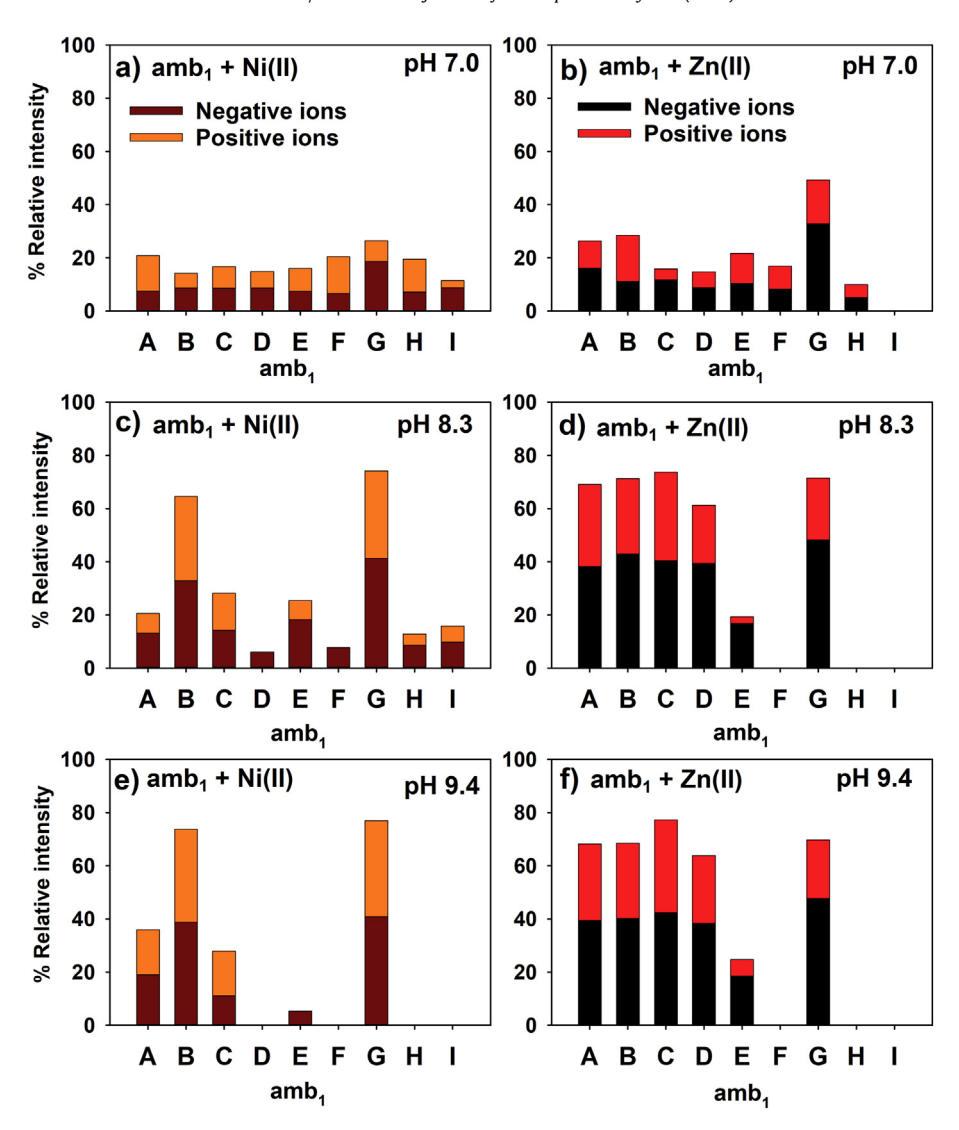


Fig. 7. The normalized relative intensities of the negatively- and positively-charged Ni(II) or Zn(II) complexes formed by the amb<sub>1</sub> species 1A, 1B, 1C, 1D, 1E, 1F, 1G, 1H and 1I at pH 7.0 a) Ni(II), b) Zn(II); pH 8.3 c) Ni(II), d) Zn(II); and pH 9.4 e) Ni(II), f) Zn(II). The relative intensities have standard deviations of 10%.

predicted that the lowest energy trans-Pro Zn(II) coordination was via the substituent groups of His<sub>1</sub>, Cys<sub>2</sub>, Cys<sub>6</sub> and the C-terminus carboxylate (Fig. S6a), analogous to the Ni(II) coordination shown in Fig. 4a. This  $[amb_{1A}-3H + Zn(II)]^-$  complex also exhibited a L-J  $CCS_{He}$  of 168  $\pm$  3 Å<sup>2</sup> in agreement with the IM-MS  $CCS_{He}$  171  $\pm$  4 Å<sup>2</sup> measured here and previously [21]. In comparison, the lowest energy conformer located for the alternate His1, Cys2, His5, and Cterminus carboxylate coordination of Zn(II) was 91 kJ/mol higher in energy (Fig. S6b) and the 2Cys-2His (Fig. S6c), which was via the imidazolate of His1, thiolates of Cys2 and Cys6 and the imidazole of His5, was 132 kJ/mol higher in free energy. When the 2His-2Cys was changed to 4Cys as for 1G the highest percent formation of the  $[amb_1-3H + Zn(II)]^-$  complex was observed, showing the importance of Cys thiolates as chelating sites. If the Cys<sub>2</sub> side group was removed, as in species 1E, the Zn(II) chelation decreased to <40% and if both Cys side groups were removed (1F, 1H, and 1I) no Zn(II) chelation was observed at pH 8.3 and 9.4.

### 3.4. Total percentage of positively- and negatively-charged Ni(II) and Zn(II) complexes

also exhibited a similar pH-dependent behavior as the negative ion analyses, although it was not as apparent as that of the negative ion analyses, probably because of excess protonation of the complexes via the positive ion electrospray process [42]. However, the results still indicated that Ni(II) and Zn(II) chelation was dependent on the weakly acidic Cys and basic His substituent groups because of the dependence on the primary structures of 1A to 1I and the increased chelation over pH 6.7 to 9.4.

Fig. 6 shows the contribution from both the positive and negative ion analyses on the relative percentage of formation of the Ni(II) and Zn(II) complexes. These results include all the amb<sub>1</sub> monomers or dimers binding one or two metals. The results show that Ni(II) was chelated most effectively by 1B and 1G at pH 8.3 and pH 9.4; which both contained the amidated C-terminus and either 2Cys-2His or 4Cys substituent groups, indicating the thiolates were most effective at chelating Ni(II) when the C-terminus was amidated. For 1G this included both the binding of a single Ni(II) and two Ni(II). Species 1A and 1C were the next highest chelators of Ni(II), at pH 8.3 and pH 9.4, and contained the His<sub>1</sub>, Cys<sub>2</sub>, Cys<sub>6</sub> and Cterminus carboxyl, providing experimental evidence of the His-2Cys-Cterm coordination of Ni(II) as shown in Fig. 4a. Species 1E formed >20% Ni(II) complexes at pH 8.3 due to the formation of an

oxidized dimer binding Ni(II), due to the formation of an intermolecular disulfide bond. Another possible Ni(II) chelation was via the deprotonated nitrogens from the backbone amide groups, but this type of coordination if it occurred was minor because **1D**, **1F**, **1H** and **1I** all exhibited < 20% formation of the Ni(II) complex, even though they had an anchoring site (His or Cys) and backbone amide groups [2].

The positive and negative ion analyses for the formation of Zn(II) complexes (Fig. 7) showed at pH 8.3 and 9.4, the Zn(II) was most effectively chelated by **1A**, **1B**, **1C**, **1D** and **1G**, which all exhibited >60% formation of Zn(II) complexes. The higher complex formation for these species indicated that the thiolates were the primary binding sites for Zn(II) chelation. Therefore, both Ni(II) and Zn(II) chelation by the  $amb_1$  peptides were dependent on the availability of the Cys substituents groups. However, the higher formation of Zn(II) complexes over Ni(II) complexes was because of the competition for the Cys forming disulfide bonds due to the likely redox activity and catalysis of Ni(II).

### 3.5. Formation of Ni(II) and Zn(II) complexes by amb $_{1A-F}$ and amb $_{5A-F}$ over pH 7.0 to 9.4

The formation of complexes for the alternative metal binding-5 (amb<sub>5</sub>) peptides (**5A** to **5F**, Fig. 1) with Ni(II) and Zn(II) have been recently published [25,27], and are compared to the formation of complexes from the **1A** to **1F** in Fig. 8. The amb<sub>5</sub> **5A** to **5F** peptides have analogous primary structures with the amb<sub>1</sub> 1A-1F, but include the addition of Tyr<sub>5</sub> in their primary structure inserted after the Pro<sub>4</sub> and before the last two amino acid residues (Fig. 1): e.g. **5A** has the primary structure ac-His-Cys-Gly-Pro-Tyr-His-Cys-OH (Fig. 1). The comparison in Fig. 8 shows the greatest selectivity for Zn(II) is from the amb<sub>5</sub> peptides, but only at pH 7.0. This indicates the addition of Tyr to the C-terminal arm is providing the extra flexibility for optimizing the positioning of the binding sites to complex the Zn(II) ion. It also suggests that the presence of the Tyr phenol group may be lowering the pKa of the 2Cys thiol groups and making the thiolates available to bind the Zn(II) at pH 7.0. At the higher pH 8.3 and pH 9.4, the formation of Zn(II) complexes increased further for both amb<sub>1</sub> and amb<sub>5</sub> and they became more equivalent in their formation. The Zn(II) chelation is especially significant for 1A, 1B, and 1C and the analogous amb<sub>5</sub> species of 5A, **5B**, and **5C**, which all contain the His<sub>1</sub>, 2Cys substituent groups and the C-terminus site predicted by B3LYP to chelate the Zn(II).

The Ni(II) binding by **5C** was most notable at pH 7.0 and the Ni(II) binding increased at pH 8.3 for **1B** and the amb<sub>5</sub> species of **5B** and **5C**. At pH 9.4, there was also increased Ni(II) binding most notably by the amb<sub>5</sub> species of **5A**, **5B** and **5C**. The higher Ni(II) binding by these amb<sub>5</sub> peptides is concomitant with a significantly lower intensity for the oxidized amb<sub>50x</sub> compared to amb<sub>10x</sub>. This indicates that the additional Tyr residue in their primary structure restricts the competition from the disulfide bond formation. However, at pH 9.4 there was the least distinction of selectivity for amb<sub>1</sub> or amb<sub>5</sub> binding Ni(II) or Zn(II), especially for species **A**, **B**, and **C**, although amb<sub>1</sub> chelation of Ni(II) was relatively low (<38%) for species **1A** and **1C**.

#### 4. Conclusions

An ESI-IM-MS study of the Ni(II), Zn(II), Co(II), Mg(II) and Ca(II) binding with a series of sequence related hexapeptides (amb<sub>1</sub> **1A-1I**) has been conducted and showed that only Ni(II) and Zn(II) will significantly bind to these peptides and in a pH-dependent manner. The Ni(II) and Zn(II) binding by amb<sub>1</sub> **1A-1I** was also compared to those of the analogous series of heptapeptides (amb<sub>5</sub> **5A-5F**) [25,27]. Both Ni(II) and Zn(II) exhibited a similar preference for the

Cys thiolate sites of the amb<sub>1</sub> and amb<sub>5</sub> peptides. The lower formation of Ni(II) complexes by amb<sub>1</sub> was due to competition from the reaction where the 2Cys sites formed a disulfide bond. Overall the amb<sub>5</sub> peptides of **5A**, **5B**, and **5C** exhibited the greatest selectivity for the formation of Zn(II) complexes at pH 7.0. At pH 8.3, the formation of Zn(II) complexes for **1A**, **1B**, **1C** and **1D** also increased. Overall the chelation of Ni(II) required a higher pH than the Zn(II) binding and was most effective at pH 9.4 by the species **1B**, **5A**, **5B** and **5C**. These ambs all contained the His<sub>1</sub>-Cys<sub>2</sub>-Cys<sub>6/7</sub> and the C-

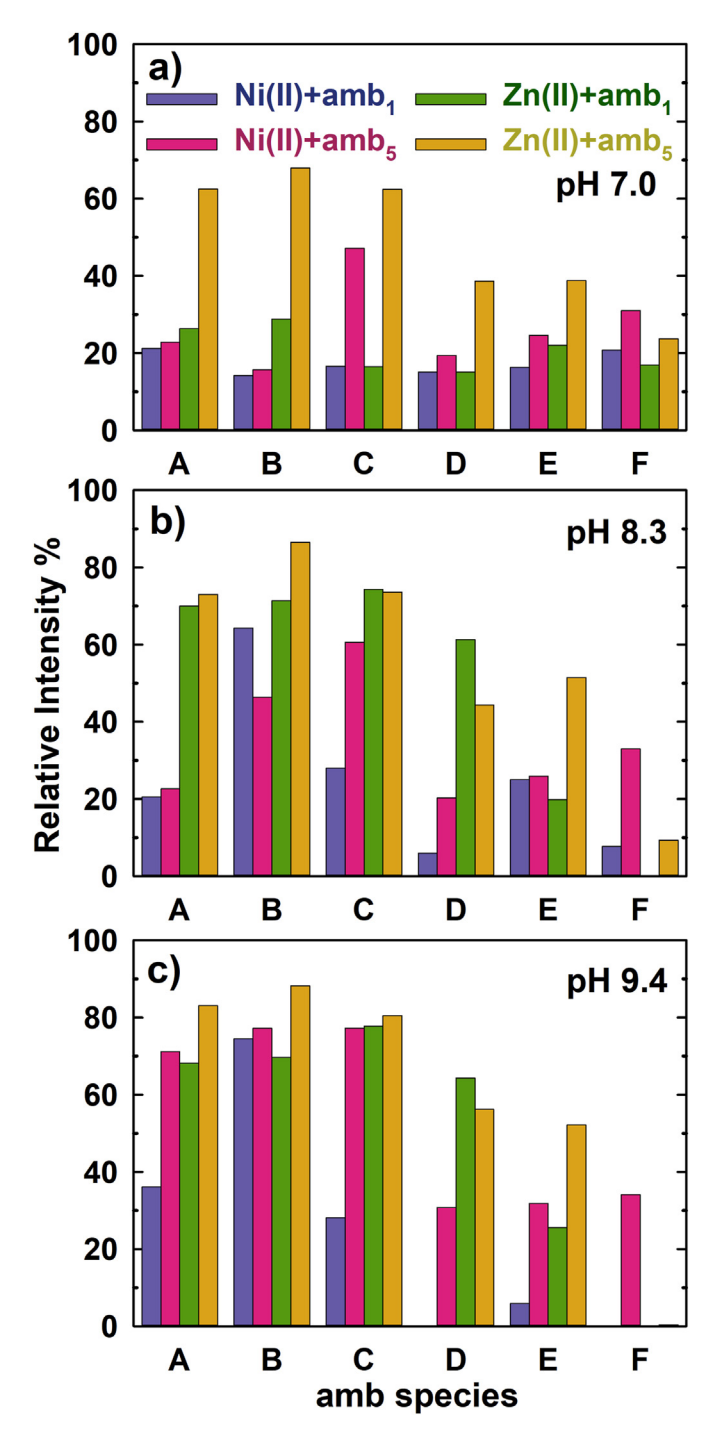


**Fig. 8.** The normalized relative intensities of the negatively- and positively-charged Ni(II) or Zn(II) complexes observed from equimolar solutions of Ni(II) or Zn(II) with amb<sub>1</sub> or amb<sub>5</sub> species **A, B, C, D, E,** and **F at a)** pH 7.0, **b)** 8.3 and **c)** 9.4. The relative intensities have standard deviations of 10%.

terminus group, which agreed with the lowest energy coordination sites of Ni(II) and Zn(II) located by the B3LYP modeling. There was also general agreement here from solution-phase studies [2] that show Zn(II) and Ni(II) will readily bind to the Cys thiolate groups and available nitrogen sites in oligopeptides, whereas, Mg(II), Ca(II) and Co(II) prefer His, Glu or Asp sites [43,44]. These results also showed that the negatively-charged complexes, measured by ESI-IM-MS, reproduced the pH-dependent chelation and protonation states that were predictable from considerations of solution-phase chemistry, suggesting that the Ni(II) and Zn(II) complexes were not significantly altered by the ESI desolvation process or by the gasphase properties of the amino acid residues. Further studies are underway on amb5 heptapeptides with new primary structures that replace one or more of the His or Cys residues with Asp, or replace the Tyr with Phe, to test their importance for selective metal ions.

### **CRediT authorship contribution statement**

**Ayobami B. Ilesanmi:** Investigation, Methodology. **Tessa C. Moore:** Investigation, Methodology. **Laurence A. Angel:** Conceptualization, Data curation, Funding acquisition, Investigation, Methodology, Project administration, Resources, Software, Supervision, Validation, Visualization, Writing - original draft, Writing - review & editing.

### **Declaration of competing interest**

The authors declare that they have no known competing financial interests or personal relationships that could have appeared to influence the work reported in this paper.

### Acknowledgements

The article is dedicated to the memory of Prof. William (Bill) L. Hase. This material is based upon work supported by the National Science Foundation under 1764436, NSF instrument support (MRI-0821247), Welch Foundation (T-0014), and computing resources from the Department of Energy (TX-W-20090427-0004-50) and L3 Communications. We thank the Bower's group of University of California - Santa Barbara for sharing the Sigma program, Jack Williams for measuring the pH of samples, and the reviewers for their help with the manuscript.

### Appendix A. Supplementary data

Supplementary data to this article can be found online at https://doi.org/10.1016/j.ijms.2020.116369.

### References

- T. Dudev, C. Lim, Competition among metal ions for protein binding sites: determinants of metal ion selectivity in proteins, Chem. Rev. 114 (1) (2014) 538–556.
- [2] I. Sovago, C. Kallay, K. Varnagy, Peptides as complexing agents: factors influencing the structure and thermodynamic stability of peptide complexes, Coord. Chem. Rev. 256 (19–20) (2012) 2225–2233.
- [3] I. Sóvágó, K. Várnagy, N. Lihi, Á. Grenács, Coordinating properties of peptides containing histidyl residues, Coord. Chem. Rev. 327–328 (2016) 43–54.
- [4] A. Choutko, W.F. van Gunsteren, Conformational preferences of a betaoctapeptide as function of solvent and force-field parameters, Helv. Chim. Acta 96 (2) (2013) 189–200.
- [5] V. Lillo, J.R. Galan-Mascaros, Transition metal complexes with oligopeptides: single crystals and crystal structures, Dalton Trans. 43 (26) (2014) 9821–9833.
- [6] Y. Berezovskaya, C.T. Armstrong, A.L. Boyle, M. Porrini, D.N. Woolfson, P.E. Barran, Metal binding to a zinc-finger peptide: a comparison between solution and the gas phase, Chem. Commun. 47 (1) (2011) 412–414.
- [7] Y. Berezovskaya, M. Porrini, C. Nortcliffe, P.E. Barran, The use of ion mobility mass spectrometry to assist protein design: a case study on zinc finger fold

- versus coiled coil interactions, Analyst 140 (8) (2015) 2847-2856.
- [8] E.M. Martin, F.D.L. Kondrat, A.J. Stewart, J.H. Scrivens, P.J. Sadler, C.A. Blindauer, Native electrospray mass spectrometry approaches to probe the interaction between zinc and an anti-angiogenic peptide from histidinerich glycoprotein, Sci. Rep. 8 (1) (2018) 8646.
- [9] L.A. Angel, Study of metal ion labeling of the conformational and charge states of lysozyme by ion mobility mass spectrometry, Eur. J. Mass Spectrom. 17 (3) (2011) 207–215.
- [10] Z. Liu, S. Chen, F. Qiao, X. Zhang, Interaction of peptide backbones and transition metal ions: 1. an IM-MS and DFT study of the binding pattern, structure and fragmentation of Pd(II)/Ni(II)-Polyalanine complexes, Int. J. Mass Spectrom. 438 (2019) 87–96.
- [11] M. Kohtani, M.F. Jarrold, S. Wee, R.A.J. O'Hair, Metal ion interactions with polyalanine peptides, J. Phys. Chem. B 108 (19) (2004) 6093–6097.
- [12] M.S. Glover, J.M. Dilger, F. Zhu, D.E. Clemmer, The binding of Ca2+, Co2+, Ni2+, Cu2+, and Zn2+ cations to angiotensin I determined by mass spectrometry based techniques, Int. J. Mass Spectrom. 354–355 (2013) 318–325.
- [13] U.K.B. Raja, S. Injeti, T. Culver, J.W. McCabe, L.A. Angel, Probing the stability of insulin oligomers using electrospray ionization ion mobility mass spectrometry, Eur. J. Mass Spectrom. 21 (6) (2015) 759–774.
- [14] Y.P. Ho, H.P. Li, L.C. Lu, Probing the interactions of oxidized insulin chain A and metal ions using electrospray ionization mass spectrometry, Int. J. Mass Spectrom. 227 (1) (2003) 97–109.
- [15] E. Sitkiewicz, M. Kloniecki, J. Poznanski, W. Bal, M. Dadlez, Factors influencing compact-extended structure equilibrium in oligomers of Aβ1-40 peptide - an ion mobility mass spectrometry study, J. Mol. Biol. 426 (15) (2014) 2871–2885.
- [16] T. Wyttenbach, D. Liu, M.T. Bowers, Interactions of the hormone oxytocin with divalent metal ions, J. Am. Chem. Soc. 130 (18) (2008) 5993–6000.
- [17] D.R. Fuller, M.S. Glover, N.A. Pierson, D.E. Clemmer, D. Kim, D.H. Russell, Cis→Trans isomerization of pro(7) in oxytocin regulates Zn(2+) binding, J. Am. Soc. Mass Spectrom. 27 (8) (2016) 1376–1382.
- [18] L. Deng, N. Sun, E.N. Kitova, J.S. Klassen, Direct quantification of protein-metal ion affinities by electrospray ionization mass spectrometry, Anal. Chem. 82 (6) (2010) 2170–2174.
- [19] J. Pan, K. Xu, X. Yang, W.-Y. Choy, L. Konermann, Solution-phase chelators for suppressing nonspecific protein-metal interactions in electrospray mass spectrometry, Anal. Chem. 81 (12) (2009) 5008–5015.
- [20] S. Zheng, S. Yuan, Z. Hou, G. Li, Y. Chen, Y. Pan, Y. Liu, G. Huang, Charge-dependent modulation of specific and nonspecific protein-metal ion interactions in nanoelectrospray ionization mass spectrometry, Rapid Commun. Mass Spectrom. 33 (19) (2019) 1502–1511.
- [21] R. Sesham, D. Choi, A. Balaji, S. Cheruku, C. Ravichetti, A.A. Alshahrani, M. Nasani, L.A. Angel, The pH dependent Cu(II) and Zn(II) binding behavior of an analog methanobactin peptide, Eur. J. Mass Spectrom. 19 (6) (2013) 463–473.
- [22] D. Choi, A.A. Alshahrani, Y. Vytla, M. Deeconda, V.J. Serna, R.F. Saenz, L.A. Angel, Redox activity and multiple copper(I) coordination of 2His-2Cys oligopeptide, J. Mass Spectrom. 50 (2) (2015) 316–325.
- [23] S.M. Wagoner, M. Deeconda, K.L. Cumpian, R. Ortiz, S. Chinthala, L.A. Angel, The multiple conformational charge states of zinc(II) coordination by 2His-2Cys oligopeptide investigated by ion mobility - mass spectrometry, density functional theory and theoretical collision cross sections, J. Mass Spectrom. 51 (12) (2016) 1120–1129.
- [24] Y. Vytla, L.A. Angel, Applying ion mobility-mass spectrometry techniques for explicitly identifying the products of Cu(II) reactions of 2his-2cys motif peptides, Anal. Chem. 88 (22) (2016) 10925–10932.
- [25] Y.-F. Lin, E.N. Yousef, E. Torres, L. Truong, J.M. Zahnow, C.B. Donald, Y. Qin, L.A. Angel, Weak acid-base interactions of histidine and cysteine affect the charge states, tertiary structure, and Zn(II)-binding of heptapeptides, J. Am. Soc. Mass Spectrom. 30 (10) (2019) 2068–2081.
- [26] E.N. Yousef, R. Sesham, J.W. McCabe, R. Vangala, L.A. Angel, Ion mobility-mass spectrometry techniques for determining the structure and mechanisms of metal ion recognition and redox activity of metal binding oligopeptides, J. Visualized Exp. 151 (2019), e60102.
- [27] E.N. Yousef, L.A. Angel, Comparison of the pH-dependent formation of His and Cys heptapeptide complexes of nickel(II), copper(II), and zinc(II) as determined by ion mobility-mass spectrometry, J. Mass Spectrom. 55 (3) (2020) e4489.
- [28] A. Malik, Y.-F. Lin, S. Pratihar, L.A. Angel, W.L. Hase, Direct dynamics simulations of fragmentation of a Zn(II)-2Cys-2His oligopeptide. Comparison with mass spectrometry collision-induced dissociation, J. Phys. Chem. 123 (32) (2019) 6868–6885.
- [29] D.W. Choi, R. Sesham, Y. Kim, L.A. Angel, Analysis of methanobactin from Methylosinus trichosporium OB3b via ion mobility mass spectrometry, Eur. J. Mass Spectrom. 18 (6) (2012) 509–520.
- [30] J.W. McCabe, R. Vangala, L.A. Ángel, Binding selectivity of methanobactin from Methylosinus trichosporium OB3b for copper(I), silver(I), zinc(II), nickel(II), cobalt(II), manganese(II), lead(II), and iron(II), J. Am. Soc. Mass Spectrom. 28 (2017) 2588–2601.
- [31] M. Whittaker, C.D. Floyd, P. Brown, A.J.H. Gearing, Design and therapeutic application of matrix metalloproteinase inhibitors, Chem. Rev. 99 (9) (1999) 2735–2776.
- [32] C. Gialeli, A.D. Theocharis, N.K. Karamanos, Roles of matrix metalloproteinases in cancer progression and their pharmacological targeting, FEBS J. 278 (1)

(2011) 16-27.

- [33] N. Borkakoti, Matrix metalloprotease inhibitors: design from structure, Biochem. Soc. Trans. 32 (1) (2004) 17–20.
- [34] P.D. Brown, Matrix metalloproteinase inhibitors, Breast Canc. Res. Treat. 52 (1–3) (1998) 215–226.
- [35] C. Amarasinghe, J.-P. Jin, The use of affinity tags to overcome obstacles in recombinant protein expression and purification, Protein Pept. Lett. 22 (10) (2015) 885–892.
- [36] S.D. Pringle, K. Giles, J.L. Wildgoose, J.P. Williams, S.E. Slade, K. Thalassinos, R.H. Bateman, M.T. Bowers, J.H. Scrivens, An investigation of the mobility separation of some peptide and protein ions using a new hybrid quadrupole/ travelling wave IMS/oa-ToF instrument, Int. J. Mass Spectrom. 261 (1) (2007) 1–12.
- [37] J.G. Forsythe, A.S. Petrov, C.A. Walker, S.J. Allen, J.S. Pellissier, M.F. Bush, N.V. Hud, F.M. Fernandez, Collision cross section calibrants for negative ion mode traveling wave ion mobility-mass spectrometry, Analyst 14 (20) (2015) 6853–6861.
- [38] F. Weigend, R. Ahlrichs, Balanced basis sets of split valence, triple zeta valence and quadruple zeta valence quality for H to Rn: design and assessment of accuracy, Phys. Chem. Chem. Phys. 7 (18) (2005) 3297–3305.
- [39] F. Weigend, Accurate Coulomb-fitting basis sets for H to Rn, Phys. Chem. Chem. Phys. 8 (9) (2006) 1057–1065.
- [40] M.J. Frisch, G.W. Trucks, H.B. Schlegel, G.E. Scuseria, M.A. Robb, J.R. Cheeseman, G. Scalmani, V. Barone, B. Mennucci, G.A. Petersson,

- H. Nakatsuji, M. Caricato, X. Li, H.P. Hratchian, A.F. Izmaylov, J. Bloino, G. Zheng, J.L. Sonnenberg, M. Hada, M. Ehara, K. Toyota, R. Fukuda, J. Hasegawa, M. Ishida, T. Nakajima, Y. Honda, O. Kitao, H. Nakai, T. Vreven, J. Montgomery, J.A., J.E. Peralta, F. Ogliaro, M. Bearpark, J.J. Heyd, E. Brothers, K.N. Kudin, V.N. Staroverov, R. Kobayashi, J. Normand, K. Raghavachari, A. Rendell, J.C. Burant, S.S. Iyengar, J. Tomasi, M. Cossi, N. Rega, J.M. Millam, M. Klene, J.E. Knox, J.B. Cross, V. Bakken, C. Adamo, J. Jaramillo, R. Gomperts, R.E. Stratmann, O. Yazyev, A.J. Austin, R. Cammi, C. Pomelli, J.W. Ochterski, R.L. Martin, K. Morokuma, V.G. Zakrzewski, G.A. Voth, P. Salvador, J.J. Dannenberg, S. Dapprich, A.D. Daniels, Ö. Farkas, J.B. Foresman, J.V. Ortiz, J. Cioslowski, D.J. Fox, Gaussian 09, Revision C.01, Gaussian, Inc., Wallingford CT, 2012.
- [41] T. Wyttenbach, G. von Helden, J.J. Batka Jr., D. Carlat, M.T. Bowers, Effect of the long-range potential on ion mobility measurements, J. Am. Soc. Mass Spectrom. 8 (3) (1997) 275–282.
- [42] H. Metwally, Q. Duez, L. Konermann, Chain ejection model for electrospray ionization of unfolded proteins: evidence from atomistic simulations and ion mobility spectrometry, Anal. Chem. 90 (16) (2018) 10069–10077.
- mobility spectrometry, Anal. Chem. 90 (16) (2018) 10069–10077.

  [43] V.V. Khrustalev, T.A. Khrustaleva, V.V. Poboinev, C.I. Karchevskaya, E.A. Shablovskaya, T.G. Terechova, Cobalt(II) cation binding by proteins, Metallomics 11 (10) (2019) 1743–1752.
- [44] T. Dudev, C. Lim, Principles governing Mg, Ca, and Zn binding and selectivity in proteins, Chem. Rev. 103 (3) (2003) 773–787.